Analytical Modeling and Simulation of Phase Noise Interference in OFDM-Based Digital Television Terrestrial Broadcasting Systems

Mohamed S. El-Tanany, Yiyan Wu, *Fellow, IEEE,* and László Házy

***Abstract*—This paper deals with the problem of modeling of phase noise in OFDM systems and the impact it may have on the bit error rate performance of such systems subject to a number of system variables and to a number of channel conditions which may be encountered when such systems are deployed for certain applications such as high speed wireless LANs and Digital Television Terrestrial Broadcasting (DTTB). The phase noise processes, the sources of which are the transmitter's and receiver's local oscillator, are modeled using what is believed to be commercially realizable phase noise masks. Such masks represent the long-time averaged power spectral densities of the local oscillator output signal.**

***Index Terms*—COFDM, digital television, DTTB, MQAM, OFDM, phase noise.**

I. Introduction

OFDM provides an effective method to mitigate intersymbol interference (ISI) in wideband signalling over multipath radio channels. The main idea is to send the data in parallel over a number of narrowband flat subchannels (see Fig. 1). This is efficiently achieved by using a set of overlapped orthogonal signals to partition the channel. A transceiver can be realized using a number of coherent QAM modems which are equally spaced in the frequency domain and which can be implemented using the IDFT on the transmitter end and the DFT on the receiving end [1]–[7]. Due to the fact that the intercarrier spacing in OFDM is relatively small, OFDM transceivers are somewhat more sensitive to phase noise by comparison to single carrier transceivers. It is the purpose of this paper to examine the impact of L.O. phase noise on the BER performance of OFDM signals over both AWGN and frequency selective channels.

The paper first discusses the relationship between the continuous time, continuous frequency L.O. phase noise model and the discrete time, discrete frequency process that is seen by the OFDM system. An analysis of the OFDM receiver is presented to assess the impact of the phase noise on the decision variables at the receiver (which are the received signal samples corrupted by noise, just before making hard decisions regarding the received data). It is then shown that the effect of phase noise on the decision variables is composed of two components: a common component which affects all data symbols equally and as such causes a sometimes visible rotation of the signal constellation, and a second component which is more like Gaussian noise and thus affects the received data points in a somewhat random manner. This representation in terms of common and foreign components has been pointed out in the literature [8]–[10]. What we introduce here that is different, is that the temporal variations of the rotational component and its dependence on the frequency spacing between the system carriers play an important role in determining the symbol-error rate performance of the OFDM system, particularly at higher operating SNR conditions. Taking the temporal variations of the rotational component of the phase noises into account, we then proceeded to derive analytical expressions for the average probability of error for 64-QAM OFDM. The resulting formulas are in a closed form which includes several integrals over the Gaussian probability curve. The analytical results are then used to quantify the impact of certain phase noise masks on the average BER performance under different SNR conditions and also subject to variations of the OFDM frame length. Computer simulation is used to treat the problem over channels with arbitrary multipath profiles and also, to investigate the impact of phase noise on channel estimation and channel equalization. The simulation model requires a user specified phase noise mask as an input. It also requires the user to identify system parameters such as sampling frequency, OFDM frame length and the size of the signal constellation.

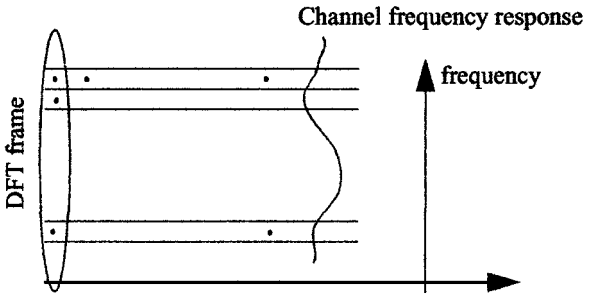

Fig. 1. Using OFDM to mitigate ISI.

II. System Description and Model

A functional block diagram of an OFDM system is shown in Fig. 2. The incoming data is fist applied to a baseband M-ary

Manuscript received January 31, 2001; revised March 14, 2001. This work was supported by the Communications Research Centre, Ottawa, Canada, under Contract 67-CRC-5-2612.

M. S. El-Tanany and L. Házy are with the Department of Systems and Computer Engineering, Carleton University, Ontario, K1S 5B6.

Y. Wu is with the Communications Research Centre, Shirley Hay, Ottawa, Ontario.

Publisher Item Identifier S 0018-9316(01)04269-X.

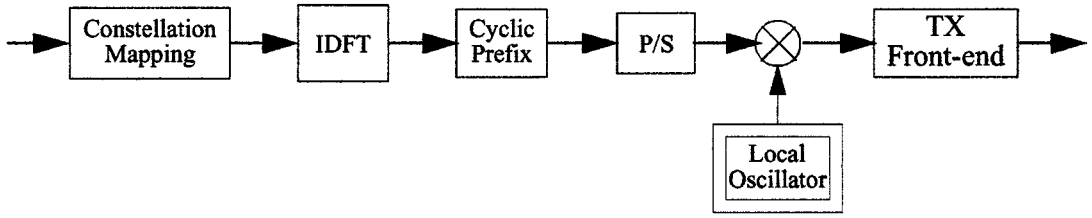

Fig. 2. Block diagram of an OFDM transmitter.

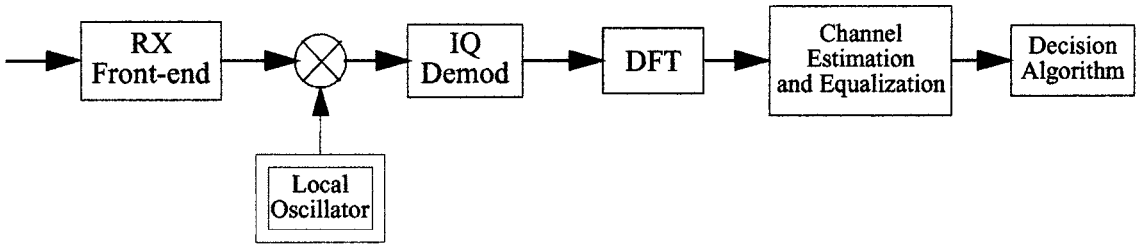

Fig. 3. Block diagram of an OFDM receiver.

QAM modulator which maps each $L = \log_2 M$ binary bits into one of the M constellation points. The M-QAM points coming out of the baseband modulator are then grouped into frames, each containing N complex constellation points. Each frame is applied to an inverse DFT processor which outputs N-complex transform coefficients. A circular prefix of length N_p is then appended to the N complex transform coefficients to form a transmitted frame which is $N+N_p$ points long. The transmitted frame is then applied to a serial-to-parallel converter and then applied to an IQ modulator to translate the spectral content of the signal to some UHF or microwave frequency band. The IQ modulation is accomplished by multiplying the complex envelope of the signal with the output of a local oscillator. This step is often accomplished at a convenient IF frequency and the modulated signal is then upconverted using a higher frequency local oscillator. For our purpose, it is sufficient to consider one local oscillator as indicated in, Fig. 2.

The local oscillator is not perfect. Its output is usually degraded due to many factors, including short term frequency drift that may in part be caused by temperature variations. The short term frequency drifts manifest themselves as phase noise which has traditionally been characterized in terms of its power spectral density.

A functional block diagram of a simplified OFDM receiver is depicted in Fig. 3. The received signal, usually corrupted by additive noise and channel distortion, is first applied to a low noise microwave front-end where it is amplified and perhaps filtered to suppress unwanted interference. The received signal is then downconverted to an IF frequency and applied to an I&Q demodulator which brings the signal down to baseband in the form in-phase and quadrature components. These in turn are applied to a A/D converter which outputs complex baseband samples at a rate of one sample per received symbol. The complex samples are then grouped into received frames which contain $N + N_p$ points each. Assuming that the frame synchronization is working, the received frames are first reduced to N points each by removing the circular prefix, and then are applied to an N-point DFT processor. The received frame is also used to estimate the frequency response of the channel. The DFT output is then equalized to generate N-decision variables which may be used to recover the data either based on threshold comparison or applied to a sequential estimation procedure such as the Viterbi algorithm.

The important block in Fig. 3 is the local oscillator, which like the transmitter local oscillator may have its own phase noise which will degrade the quality of the received signal and the overall BER performance. For analog TV (ATV) applications the Tx local oscillator is of much better spectral purity since this exists only in the base station and as such it does not have to be very economical. The Rx local oscillator signal on the other hand is provided with a cheap commercial TV tuner which exhibits high levels of phase noise. It is for this reason that we will concentrate on the Rx LO phase noise without explicit mention of the Tx LO phase noise. It should however be mentioned that the analysis we will develop can still be applied to cases where the phase noise is introduced by a combination of both local oscillators.

III. Phase Noise Analysis

Let $\varphi(\mathrm{t})$ represent tile analog (i.e., continuous time and frequency) phase noise process of the local oscillator which will be assumed Gaussian with zero mean and power spectral density specified by some phase noise mask. As such, $\varphi(\mathrm{t})$ can be written as follows:

$$\varphi(\mathrm{t}) = \mathrm{h}(\mathrm{t}) \otimes \mathrm{n}(\mathrm{t}) \tag{1}$$

where $\mathrm{h}(\mathrm{t})$ is the impulse response of a low-pass linear filter whose frequency response is given by:

$$|\mathrm{H}(\mathrm{f})|^2 = \psi(\mathrm{f}) \times \text{scale factor} \tag{2}$$

where $\psi(\mathrm{f})$ is the phase noise mask of the local oscillator and $\mathrm{n}(\mathrm{t})$ is a white Gaussian noise process with power spectral

density N_0. By definition, the autocorrelation function of the phase noise process is given by:

$$R_\varphi(\tau) = \int_{-\infty}^{\infty} \psi(f) e^{j2\pi f\tau}\, df \tag{3}$$

which can also be written in terms of $h(t)$ as follows:

$$R_\varphi(\tau) = \int_{-\infty}^{\infty} N_0 h^*(t-\tau) h(t) e^{j2\pi f\tau}\, dt. \tag{4}$$

We are interested in the autocorrelation function of the sampled phase-noise process. This is defined by:

$$R_\varphi(i, j) = \langle \varphi(iT)\varphi(jT)\rangle \equiv \langle \varphi_i \varphi_j\rangle \tag{5}$$

where

$$\varphi(iT) = \int_{-\infty}^{\infty} h(\tau) n(iT-\tau)\, d\tau \tag{6}$$

and therefore

$$\begin{aligned} R_\varphi(i, j) &= \int_{-\infty}^{\infty}\int_{-\infty}^{\infty} h(\tau_1) h^*(\tau_2) \langle n(iT-\tau_1) n(jT-\tau_2)\rangle \\ &\quad \cdot (d\tau_1)(d\tau_2) \\ &= N_0 \int_{-\infty}^{\infty}\int_{-\infty}^{\infty} h(\tau_1) h^*(\tau_2) \delta(iT - jT + \tau_2 - \tau_1) \\ &\quad \cdot (d\tau_1)\, d\tau_2 \end{aligned} \tag{7}$$

which can be rewritten as

$$R_\varphi(i, j) = N_0 \int_{-\infty}^{\infty} h(\tau_2 - (j-i)T) h^*(\tau_2)\, d\tau_2. \tag{8}$$

From (8) and (3) and (4) the discrete autocorrelation function can be rewritten in terms of the continuous phase noise power spectral density as follows:

$$\begin{aligned} R_\varphi(1, m) &= \int_{-\infty}^{\infty} \psi(f) e^{j(1T - mT)2\pi f}\, df \\ &= \int_{-\infty}^{\infty} \psi(f) e^{j(1-m)2\pi(f/f_s)}\, df. \end{aligned} \tag{9}$$

In order to simplify the analysis that follows we make the assumptions:

- the communication channel is additive white Gaussian
- the channel frequency response is flat
- the phase noise variance is very small compared to unity, in which case the assumption that $e^{j\varphi(t)} \cong 1 + j\varphi(t)$ can be invoked.

Subject to the above, the input to the DFT block during one OFDM frame interval may be written as:

$$x(i) = A(i) \times e^{j\varphi(iT)} \qquad i = 1 \text{ to } N-1 \tag{10}$$

where $\{A(i)\}$ are the IDFT coefficients of the QAM symbol sequence $\{a(i)\}$ and T is the sampling period. With the approximating assumptions made above, $x(i)$ can be rewritten:

$$x(i) \cong A(i) + jA(i)\varphi(iT) \tag{11}$$

and the output of the DFT block can therefore be written as

$$Y(k) = \left(\alpha_k + j\frac{1}{N}\alpha_k \Phi_0\right) + j\frac{1}{N}\left(\sum_{i\neq k} \alpha_i \Phi(k \oplus i)\right). \tag{12}$$

By examining (12) it becomes clear that the phase noise disturbs the decision variables in two ways:

- The first bracketed component to the right implies a phase rotation in the amount Φ_0/N for all the received data symbols in the current OFDM frame. This is a common rotation and it results in a rotation of the entire signal constellation. We will use N_c to denote this common rotation factor, that is

$$N_c = \frac{\Phi_0}{N} = \frac{1}{N}\sum_{n=0}^{N-1} \varphi(n). \tag{13}$$

- The second bracketed component depends on the data symbols within the current frame. Assuming that the frame is relatively large and that the data points are statistically independent, it can then be argued that the result is a Gaussian process which is likely to affect the decision variables in the same way additive Gaussian noise does. This second component has been referred to in the literature as a foreign component, but here it will be referred to as a dispersive component due to the way it affects the received signal constellation. We will use N_f to denote this second term, that is

$$N_f = j\frac{1}{N}\sum_{i\neq k} \alpha_i \Phi(k \oplus i). \tag{14}$$

The common component is linearly related to the sampled phase noise process and as a result, N_c is Gaussian with a mean and variance given by:

$$\langle N_c\rangle = \frac{1}{N}\sum_{n=0}^{N-1} \langle \varphi(n)\rangle = 0 \tag{15}$$

$$\begin{aligned} \langle |N_c|^2\rangle &= \left\langle \left(\frac{1}{N}\sum_n \varphi(n)\right)^2 \right\rangle \\ &= \frac{1}{N^2}\sum_m \sum_n \langle \varphi(n)\varphi^*(m)\rangle \end{aligned} \tag{16}$$

$$\begin{aligned} \langle |N_c|^2\rangle &= \int_{-\infty}^{\infty} \frac{\psi(f)}{N^2}\left(\sum_m\sum_n e^{(j2\pi(n-m)f)/f_s}\right) df \\ &= \int_{-\infty}^{\infty} \frac{\psi(f)}{N^2}\left|\frac{sin((\pi N f)/f_s)}{sin((\pi f)/f_2)}\right|^2 df. \end{aligned} \tag{17}$$

The foreign dispersive component is also Gaussian with zero mean and variance which is evaluated next. The variance of the sum of the rotational and the dispersive components is equal to the sum of the variances of both components. As such, the variance of the dispersive component can be easily obtained if we know the variance of the sum. This is given by:

$$\begin{aligned} \sigma_s^2 &= \frac{1}{N^2}\left\langle \sum_l \sum_m \alpha_l \alpha_m^* \Phi(k-l)\Phi^*(k-m)\right\rangle \\ &= \frac{1}{N^2}\sum_l\sum_m \langle \alpha_l \alpha_m^*\rangle \langle \Phi k - l \Phi^* k - m\rangle. \end{aligned} \tag{18}$$

In other words,

$$\sigma_s^2 = \frac{\alpha^{-2}}{N^2}\sum_l \langle |\Phi(l)|^2\rangle \tag{19}$$

where

$$\langle|\Phi(\mathrm{k})|^2\rangle = \left\langle \sum_{\mathrm{n}} \sum_{\mathrm{m}} \varphi(\mathrm{n})\varphi^*(\mathrm{m}) \mathrm{e}^{-\mathrm{j}2\pi \mathrm{nk/N}} \mathrm{e}^{\mathrm{j}2\pi \mathrm{mk/N}} \right\rangle = \sum_{\mathrm{n}} \sum_{\mathrm{m}} \langle \varphi(\mathrm{n})\varphi^*(\mathrm{m})\rangle \mathrm{e}^{-\mathrm{j}2\pi(\mathrm{n-m})\mathrm{k/N}} \tag{20}$$

and which can be rewritten as

$$\langle|\Phi(\mathrm{k})|^2\rangle = \sum_{\mathrm{n}} \sum_{\mathrm{m}} \mathrm{e}^{-\mathrm{j}2\pi(\mathrm{n-m})\mathrm{k/N}} \cdot \int_{-\infty}^{\infty} \psi(\mathrm{f}) \mathrm{e}^{\mathrm{j}2\pi \mathrm{f}(\mathrm{n-m})\mathrm{T}} \,\mathrm{df}. \tag{21}$$

Therefore, we get

$$\langle|\Phi(\mathrm{k})|^2\rangle = \int_{-\infty}^{\infty} \psi(\mathrm{f}) \left(\sum_{\mathrm{n}} \mathrm{e}^{\mathrm{j}2\pi(\mathrm{f/f_s} - \mathrm{k/N})\mathrm{n}} \right) \cdot \left(\sum_{\mathrm{m}} \mathrm{e}^{-\mathrm{j}2\pi(\mathrm{f/f_s} - \mathrm{k/N})\mathrm{m}} \right) \mathrm{df} \tag{22}$$

and

$$\sigma_{\mathrm{s}}^2 = \frac{\alpha^{-2}}{\mathrm{N}^2} \sum_{\mathrm{k}} \int_{-\infty}^{\infty} \psi(\mathrm{f}) \left| \frac{sin\pi\left(\dfrac{\mathrm{f}}{\mathrm{f_s}} - \dfrac{\mathrm{k}}{\mathrm{N}}\right)\mathrm{N}}{sin\pi\left(\dfrac{\mathrm{f}}{\mathrm{f_s}} - \dfrac{\mathrm{k}}{\mathrm{N}}\right)} \right| \mathrm{df} = \alpha^{-2} \int_{-\infty}^{\infty} \psi(\mathrm{f})\,\mathrm{df} \tag{23}$$

where α^{-2} is the average signal power. We conclude that the variance of the sum of the two noise components normalized to the signal power is equal to the area under the phase noise mask. The variance of the dispersive component is therefore given by $\sigma_f^2 = \sigma_s^2 - \sigma_c^2$.

We now summarize the important points in this section. The decision variables which are represented by the output of the DFT block in the receiver block diagram of Fig. 3 are corrupted by the phase noise process in two different ways:

First, the entire signal constellation is rotated by an amount N_c which is a zero mean Gaussian process with variance given by

$$\sigma_{\mathrm{c}}^2 = \int_{-\infty}^{\infty} \frac{\psi(\mathrm{f})}{\mathrm{N}^2} \left| \frac{sin((\pi \mathrm{Nf})/\mathrm{f_s})}{sin((\pi \mathrm{f})/\mathrm{f_s})} \right|^2 \mathrm{df} \tag{24}$$

where

- N represents the OFDM frame length,
- f_s represents the sampling frequency and
- $\psi(\mathrm{f})$ is the power spectral density of the local oscillator's phase noise process.

It should be noted here that $\psi(f)$ is in reality a band-limited process with a bandwidth less than half of the sampling rate. Therefore, the integration limits in (24) can be changed to the range $-fs/2 \cdots f_s/2$. Assuming that f_s is held constant, the variance σ_c^2 is a monotonically decreasing function of N. It reaches a maximum for $\mathrm{N} = 1$ and approaches zero as N approaches infinity. This implies that OFDM systems which use shorter frame lengths will experience larger constellation rotations while systems with very large frames exhibit much smaller rotation.

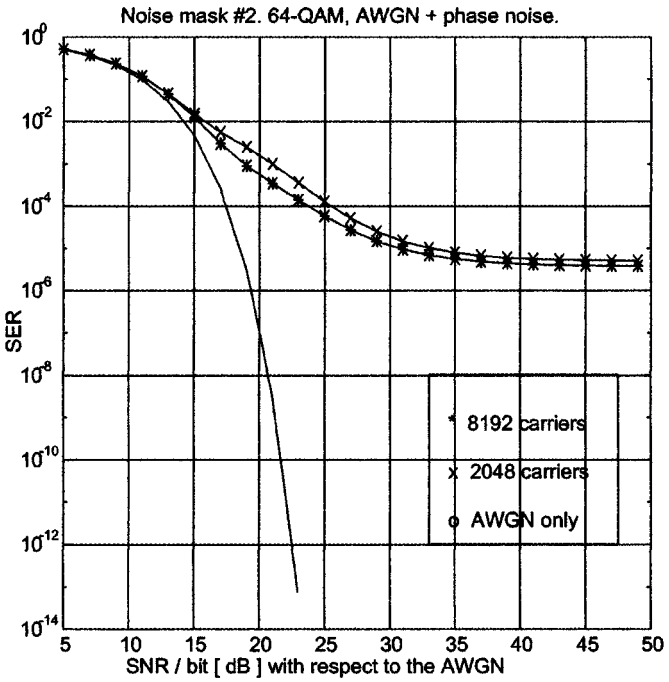

Fig. 4. Analytical results showing the symbol error rate as a function of SNR/bit.

The decision variables are also corrupted by a dispersive noise component that is essentially Gaussian with zero mean and variance

$$\sigma_{\mathrm{f}}^2 = \int_{-\mathrm{f_s}/2}^{\mathrm{f_s}/2} \psi(\mathrm{f})\,\mathrm{df} - \int_{-\mathrm{f_s}/2}^{\mathrm{f_s}/2} \frac{\psi(\mathrm{f})}{\mathrm{N}^2} \left| \frac{sin((\pi \mathrm{Nf})/\mathrm{f_s})}{sin((\pi \mathrm{f})/\mathrm{f_s})} \right|^2 \mathrm{df}. \tag{25}$$

We notice that σ_{f}^2 is a monotonically increasing function of N with a minimum of zero as $\mathrm{N} = 1$ (i.e., for a single carrier system). If left uncompensated, the rotational component can severely impact the BER performance of the OFDM system. The impact of this component on the average BER performance of M-QAM OFDM for $\mathrm{M} = 16$ and $\mathrm{M} = 64$ is analyzed in the following section.

IV. Probability of Error Analysis

The conditional BER performance (conditioned on the rotational component) for 16-QAM OFDM and for 64-QAM OFDM for a given value of the rotational noise component N_c is derived in the Appendix and it can be written as follows:

$$\begin{aligned} \mathrm{P_e}|_{16\mathrm{QAM}} &= \overline{\mathrm{P_e}} + \tfrac{3}{4}\left[(\Delta_1^1 - \Delta_2^1) + (\Delta_1^3 - \Delta_2^3)\right] \\ \mathrm{P_e}|_{64\mathrm{QAM}} &= \overline{\mathrm{P_e}} + \tfrac{7}{16}\left[(\Delta_1^1 - \Delta_2^1) + (\Delta_1^3 - \Delta_2^3) + (\Delta_1^5 - \Delta_2^5) + (\Delta_1^7 - \Delta_2^7)\right] \end{aligned} \tag{26}$$

where

$$\begin{aligned} \Delta_1^1 &= \int_{(\delta/\sigma_{\mathrm{f}})(1-\mathbf{l}\cdot\mathbf{n_c})}^{\delta/\sigma_{\mathrm{f}}} \frac{1}{\sqrt{2\pi}} \mathrm{e}^{-\eta^2/2}\,\mathrm{d}\eta \\ \Delta_2^1 &= \int_{\delta/\sigma_{\mathrm{f}}}^{(\delta/\sigma_{\mathrm{f}})(1+\mathbf{l}\cdot\mathbf{n_c})} \frac{1}{\sqrt{2\pi}} \mathrm{e}^{-\eta^2/2}\,\mathrm{d}\eta \end{aligned} \tag{27}$$

$$\delta|_{16\mathrm{QAM}} = \sqrt{\frac{\mathrm{E_{av}}}{\mathrm{T_s}} \times \frac{3}{2\cdot(16-1)}} = \sqrt{\frac{\mathrm{E_{av}}}{10\cdot \mathrm{T_s}}}$$

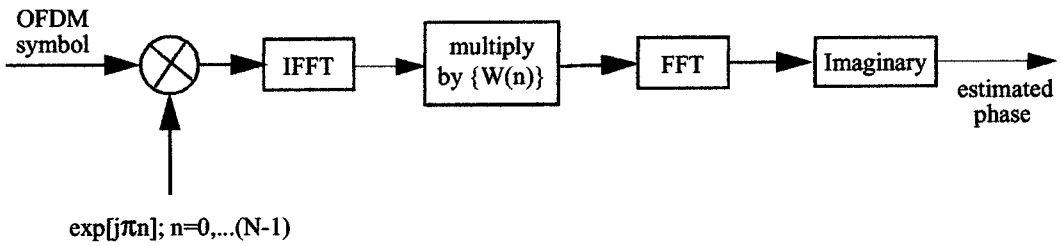

Fig. 5. Carrier recovery processing steps.

$$\delta|_{64\mathrm{QAM}} = \sqrt{\frac{\mathrm{E_{av}}}{\mathrm{T_s}} \times \frac{3}{2\cdot(64-1)}} = \sqrt{\frac{\mathrm{E_{av}}}{42\cdot \mathrm{T_s}}}. \quad (28)$$

Therefore,

$$\left.\frac{\delta}{\sigma_\mathrm{f}}\right|_{16\mathrm{QAM}} = \sqrt{\frac{\mathrm{E_{av}}/\sigma_\mathrm{f}^2}{10\cdot \mathrm{T_s}}} = \sqrt{\frac{\mathrm{SNR}}{10}}$$
$$\left.\frac{\delta}{\sigma_\mathrm{f}}\right|_{64\mathrm{QAM}} = \sqrt{\frac{\mathrm{E_{av}}/\sigma_\mathrm{f}^2}{42\cdot \mathrm{T_s}}} = \sqrt{\frac{\mathrm{SNR}}{42}}. \quad (29)$$

The average symbol error probability is obtained by averaging the, conditional probability of (26) over the distribution of the rotational component. This component is Gaussian with zero mean and variance given by (24).

V. Variance of the Rotational Component

The phase noise process of commercial tuners is often described in terms of a phase noise mask which is piecewise linear and has units of dBc/Hz. We will use $\nu(\mathrm{f})$ to denote such a mask. Phase noise masks can be fully described in terms of the coordinates of their breakpoints. Using these coordinates and the fact that the mask is piecewise linear we can compute the phase noise spectrum in absolute units as follows:

$$\nu(\mathrm{f}) = \frac{\eta_\mathrm{i}\lambda_{\mathrm{i}+1} - \eta_{\mathrm{i}+1}\lambda_\mathrm{i}}{\lambda_{\mathrm{i}+1} - \lambda_\mathrm{i}} + \mathrm{f}\frac{\eta_{\mathrm{i}+1} - \eta_\mathrm{i}}{\lambda_{\mathrm{i}+1} - \lambda_\mathrm{i}} \quad (30)$$

$$\nu(\mathrm{f}) = 10\cdot\log\frac{\psi(\mathrm{f})}{\mathrm{P_{car}}} \quad (31)$$

$$\psi_\mathrm{i}(\mathrm{f}) = \mathrm{P_{car}} \times 10^{\left[\frac{1}{10}\left(\frac{\eta_\mathrm{i}\lambda_{\mathrm{i}+1}-\eta_{\mathrm{i}+1}\lambda_\mathrm{i}}{\lambda_{\mathrm{i}+1}-\lambda_\mathrm{i}} + \mathrm{f}\frac{\eta_{\mathrm{i}+1}-\eta_\mathrm{i}}{\lambda_{\mathrm{i}+1}-\lambda_\mathrm{i}}\right)\right]} \quad (32)$$

$$\sigma_\mathrm{c}^2 = \sum_{\mathrm{i}=1}^{\mathrm{L}} \int_{\lambda_\mathrm{i}}^{\lambda_{\mathrm{i}+1}} \frac{\psi_\mathrm{i}(\mathrm{f})}{\mathrm{P_{car}}} \left|\frac{sin((\pi \mathrm{fN})/\mathrm{f_s})}{sin((\pi \mathrm{f})/\mathrm{f_s})}\right|^2 \mathrm{df} \quad (33)$$

$$\sigma_\mathrm{f}^2 = \sum_{\mathrm{i}=1}^{\mathrm{L}} \int_{\lambda_\mathrm{i}}^{\lambda_{\mathrm{i}+1}} \frac{\psi_\mathrm{i}(\mathrm{f})}{\mathrm{P_{car}}} \mathrm{df} - \sigma_\mathrm{c}^2. \quad (34)$$

The average probability of symbol errors for a 64-QAM signal has been calculated according to the procedure outlined above with the results shown in Fig. 7. These results are based on a phase noise mask with break-points at 1 kHz and 200 kHz. The average power of the phase noise process is about 29 dB below the carrier. Fig. 7 suggests that:

- The effect of phase noise on SER performance is negligible for relatively low SNR (below 12 dB).
- The performance degradation increases rapidly as the SNR/bit increases beyond 25 dB. This is due to the presence of an irreducible error floor. The impact on the 8k and 2k frame sizes is about the same since no attempt has been made to compensate for phase noise in either case. The SNR degradation due to phase noise, at an error rate of 10^{-4}, is about 3 dB.

VI. Carrier Recovery

Carrier recovery refers to the estimation of, and compensation for the phase noise sequence $\{\varphi(0), \varphi(1)\cdots\varphi(N-1)\}$ across an OFDM frame. This task can be accomplished with the aid of at least one CR (carrier recovery) pilot tone. The design of the CR pilot differs from the channel estimation pilots in that a frequency guard interval is mandatory on both sides of the CR pilot to make possible the extraction of the prominent phase noise sidebands with as little interference from the data symbols as possible. The selection of the frequency guard interval is obviously dependent on the shape of the phase noise spectral mask.

For the sake of simplicity, we shall assume that the carrier recovery is achieved using an ideal bandpass filter with its passband centered on the CR pilot-tone frequency. This filtering operation is to be performed in the frequency domain using the FFT and IFFT. The frequency guard interval normalized to the OFDM tone spacing will be denoted by G, and the CR filter bandwidth normalized to the OFDM tone spacing is denoted B. The CR pilot tone normalized frequency is taken as $N/2$.

The processing steps involved in the carrier phase recovery are illustrated in Fig. 5. The window function $W(n)$ is a rectangular window which is equal to unity for $n = 0\cdots B/2$ and for $n = N - B/2\cdots N-1$, and is zero otherwise.

The output of the carrier recovery subsystem in Fig. 5 consists of three components:

1) A desired component which is directly dependent on the phase noise sidebands within a bandwidth B. This component is of the form

$$\mathrm{x_{d(n)}} = \Phi(0) + 2|\Phi(\mathrm{I})|cos\left(2\pi\frac{\mathrm{n}}{\mathrm{N}}\right) + 2|\Phi(2)|cos\left(2\pi\frac{2\mathrm{n}}{\mathrm{N}}\right) + \cdots + 2\left|\Phi\left(\frac{\mathrm{B}}{2}-1\right)\right| cos\left(2\pi\frac{(\mathrm{B}/2-1)\mathrm{n}}{\mathrm{N}}\right) \quad (35)$$

with a variance equal to

$$\sigma_\mathrm{d}^2 = \mathrm{a_c^2}\left[|\Phi(0)|^2 + 2|\Phi(1)|^2 + \cdots + 2\left|\Phi\left(\frac{\mathrm{B}}{2}-1\right)\right|^2\right]. \quad (36)$$

2) An interfering component caused by interference from the information bearing OFDM tones as a result of tone spreading that is created by the phase noise process. The

variance of this information related interference is given by

$$\sigma_{\mathrm{i}}^2 = 2 \sum_{\mathrm{i=N/2+G}}^{\mathrm{N-1}} \mathrm{E}[|\mathrm{a_i}|^2]|\xi_{\mathrm{i}}|^2 \tag{37}$$

where

$$|\xi_{\mathrm{i}}|^2 = \sum_{\mathrm{k=i-N/2-B/2}}^{\mathrm{i-N/2+B/2}} |\Phi(\mathrm{k})|^2 \cong \mathrm{B}|\Phi(\mathrm{i}-\mathrm{N}/2)|^2. \tag{38}$$

3) An interfering component caused by the additive thermal noise in the system and which has a variance of the form

$$\sigma_{\mathrm{n}}^2 = \sigma_{\mathrm{a}}^2 \mathrm{B} \frac{1}{\mathrm{SNR_t}} \tag{39}$$

where $\mathrm{SNR_t}$ is the average signal-to-noise ratio per tone and σ_{a}^2 is the average symbol power.

The normalized mean-square error of the recovered carrier can therefore be written as

$$\begin{aligned}\mathrm{NMSE} &= \frac{\mathrm{B}\sigma_{\mathrm{a}}^2 \sum_{\mathrm{i=N/2+G}}^{\mathrm{N-1}} |\Phi(\mathrm{i})|^2 + \sigma_{\mathrm{a}}^2 \mathrm{B} \frac{1}{\mathrm{SNR_t}}}{|\mathrm{a_c^2}| \left[|\Phi(0)|^2 + 2 \sum_{\mathrm{i=1}}^{\mathrm{B/2}} |\Phi(\mathrm{i})|^2 \right]} \\ &= \left[\frac{\mathrm{B}\sigma_{\mathrm{a}}^2}{|\mathrm{a_c}|^2} \right] \times \frac{2 \sum_{\mathrm{i=G}}^{\mathrm{N/2-1}} |\Phi(\mathrm{i})|^2 + \frac{1}{\mathrm{SNR_t}}}{\left[|\Phi(0)|^2 + 2 \sum_{\mathrm{i=1}}^{\mathrm{B/2}} |\Phi(\mathrm{i})|^2 \right]}. \end{aligned} \tag{40}$$

The first factor in the numerator of (40), namely $2 \cdot \sum_{\mathrm{i=N/2+G}}^{\mathrm{N-1}} |\Phi(\mathrm{i})|^2$ is recognized as the power of the phase noise process falling outside a bandwidth equal to the frequency guard interval and as such, it decreases monotonically with G. This component also increases with the number of points in an OFDM frame (i.e., the FFT size N). The second term in the numerator accounts for the additive white Gaussian noise disturbance to the recovered phase noise sequence. The denominator of the second factor in (40) represents the phase noise power (desired component) measured within the CR filter bandwidth.

As an example, let us consider the phase noise mask shown in Fig. 6. Assume that this mask represents the LO phase noise in an OFDM system which utilizes a N-point FFT. From (40) above we calculated the CR normalized MSE as a function of the CR filter bandwidth relative to the OFDM signal tone spacing, with the frequency guard interval as a parameter. The result is a family of curves as illustrated in Figs. 7–9.

From Figs. 7 and 9 we notice that under high SNR conditions the normalized MSE has an irreducible value caused by the first term in the numerator of (40). This value increases as the frequency guard interval is reduced. The curves also suggest that there is an optimum value for the CR filter bandwidth.

Fig. 8 presents the results for an additive noise SNR of 30 dB, which is approximately the value needed for an error rate of 10^{-6} assuming 64-QAM modulation is used. This set of curves exhibits a similar trend as observed in Figs. 7 and 9, except that now the sensitivity of the normalized MSE to the frequency guard interval is reduced. It is worthy noting that the numerical results shown above are based on the assumption that the CR pilot power is equal to 1.5% of the OFDM signal power.

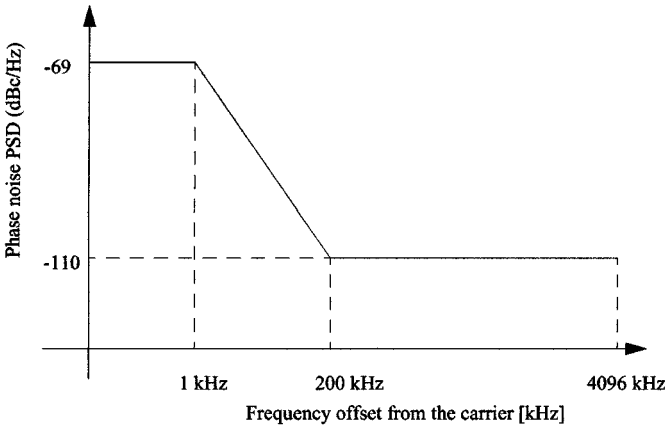

Fig. 6. An example phase noise mask (used in many computations to follow).

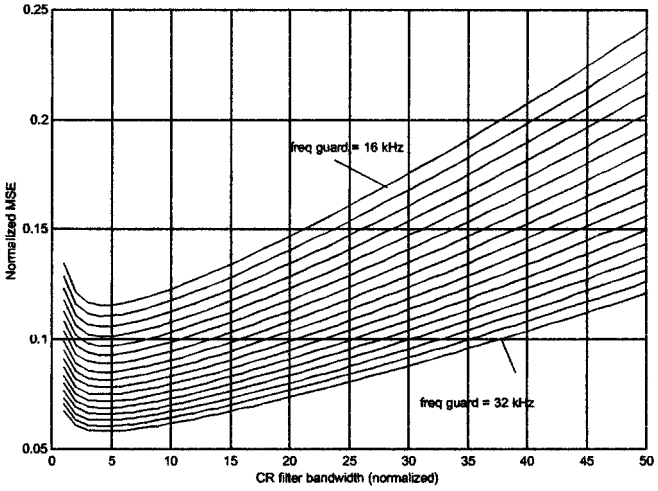

Fig. 7. Normalized MSE under high SNR conditions, for a 8192 FFT system.

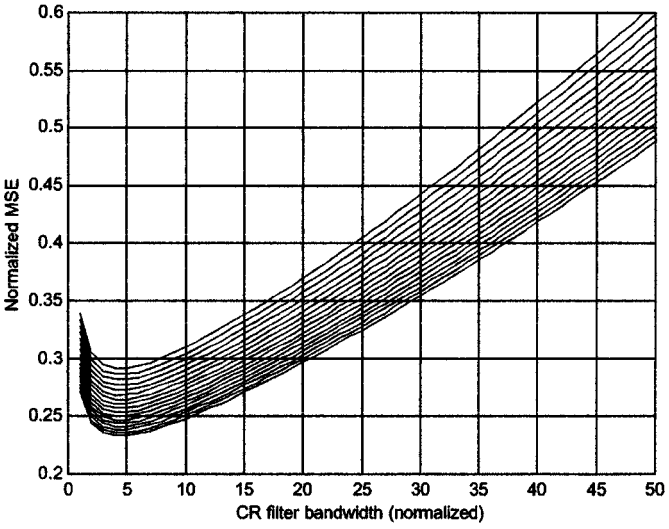

Fig. 8. Normalized MSE for a SNR = 30 dB, for a 8192 FFT system.

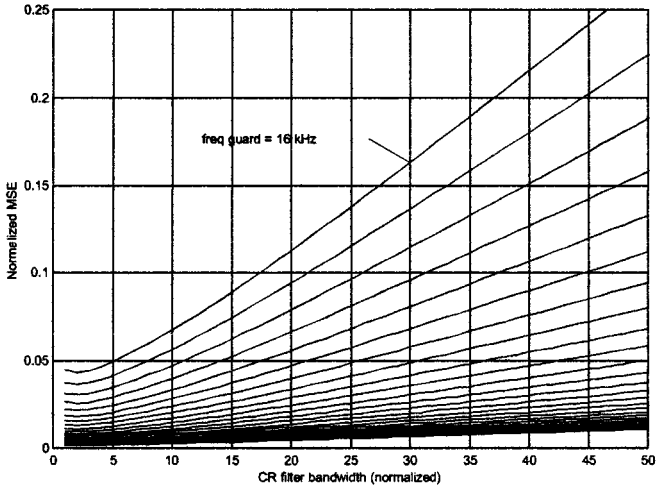

Fig. 9. Normalized MSE under high SNR conditions, for a 2048 FFT system.

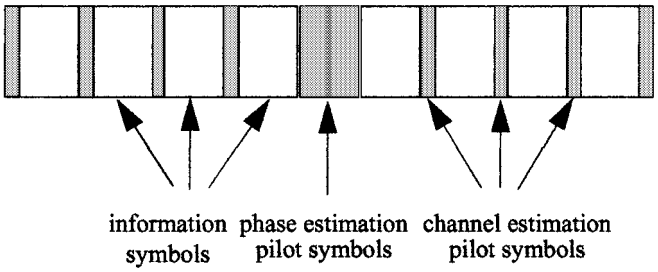

Fig. 10. OFDM frame format.

In summary, the analysis given in this section can be used to identify benchmarks for the necessary frequency guard interval required around the CR pilot, and also to identify a benchmark for the carrier recovery filter bandwidth.

VII. Simulation

In order to quantify the effect of phase noise on OFDM over channels with frequency selective responses we had to resort to simulation. Our model assumes M-QAM modulation. No forward error correction is assumed in the model. The transmitted OFDM frame structure is shown in Fig. 10.

Several equally spaced pilots are used for channel estimation purposes and a carrier recovery pilot is inserted in the middle of the frame with a guard band on both sides. The number of pilots used and their relative power levels (compared to the data subscribers) are user selectable. The OFDM frame size is also selectable, but we are going to discuss results for frame sizes of 8k and 2k carriers only.

Fig. 11 illustrates the frequency domain picture of the transmitted signal. The larger peaks represent channel estimation pilots, and the carrier recovery estimation pilot.

Fig. 12 is a functional diagram for the main processing functions of the OFDM receiver used for simulation.

The received signal is first processed to estimate the received phase noise process using the carrier phase pilot. The carrier recovery bandwidth was found to be an important parameter and as a result it is user selectable. The baseband signal is multiplied by the complex conjugate of the estimated phase noise vector.

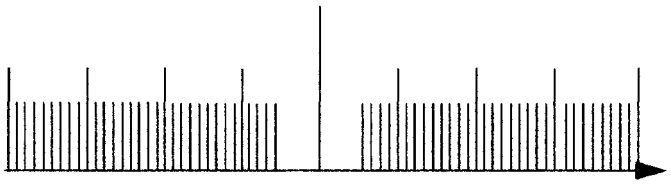

Fig. 11. Illustration of the power spectral density of an OFDM frame.

The compensated signal is also processed to extract an estimate of the frequency response of the channel based on the channel estimation pilots. The estimated channel response is used to equalize the phase-compensated signal frame. Automatic gain control is performed and finally the baseband signal is applied to a slicer to recover the received data symbols.

A. Results

Fig. 13 shows the symbol error rate as a function of the symbol energy to noise density ratio. These results are based on the simulation of an 8k OFDM system. The phase noise mask used here is similar to the one shown in Fig. 6 except that the break points are at 2 kHz and 100 kHz. From Fig. 13 it is clear that:

- The SER performance degradation due to channel estimation errors is negligible (in this case the CE pilots are relatively high at 10 dB above the average energy per information symbol).
- Performance degradation at SER $= 10^{-4}$, as caused by phase noise, is about 3 dB relative to the performance of an ideal system.
- Phase estimation and compensation using the CR algorithm shown in Fig. 5 results in an SER performance that is within 0.6 dB from ideal.

Fig. 14 shows the symbol error rate as a function of the symbol energy to noise density ratio. These results are based on the simulation of an 8k OFDM system The phase noise mask used here is identical to that shown in figure. From Fig. 14 it is clear that:

- The SER performance degradation due to channel estimation errors is slightly higher by comparison to the case of Fig. 13.
- Performance degradation at SER $= 10^{-4}$, as caused by phase noise, is about 3 dB relative to the performance of an ideal system. This is identical to the value observed in Fig. 13.
- Phase estimation and compensation using the CR algorithm shown in Fig. 5 results in an SER performance that is within 1 dB from ideal. This is higher than the 0.6 dB observed in Fig. 13.

Fig. 15 shows the symbol error rate as a function of the symbol energy to noise density ratio. These results are based on the simulation of an 2k OPDM system. The phase noise mask used here is identical to the one used in Fig. 6. From Fig. 15 it is clear that:

- The SER performance degradation due to channel estimation errors is lower than the degradation shown in the 8k OFDM case of Fig. 14.

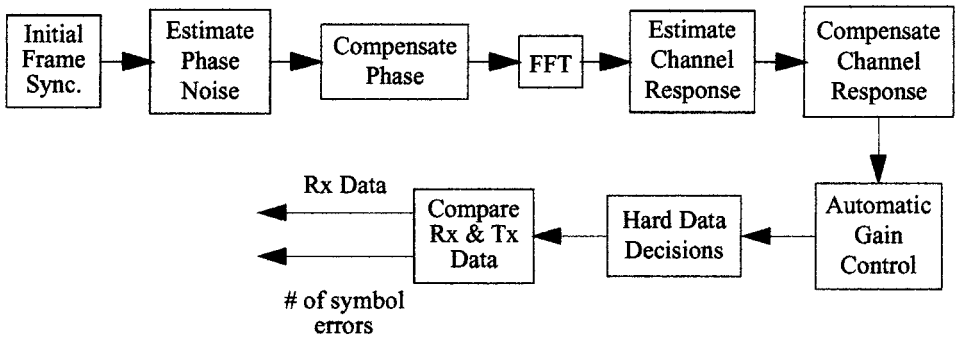

Fig. 12. Functional diagram of the simulated OFDM receiver.

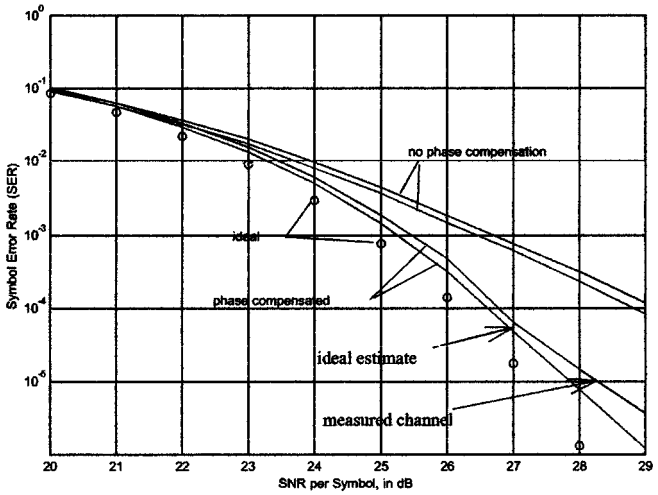

Fig. 13. SER performance of an 8192-tone OFDM system in the presence of phase noise over flat channels. This system uses 128 CE pilots at 6 dB relative to the corner points of the 64-QAM constellation. The phase noise mask break points are at 2 kHz and 100 kHz. The average phase noise power is -29 dB relative to the carrier.

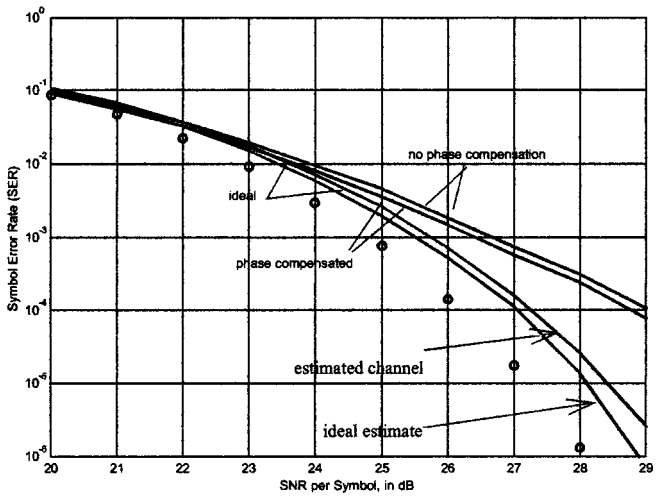

Fig. 14. SER performance of an 8192-tone OFDM system in the presence of phase noise over flat channels. This system uses 128 CE pilots at 6 dB relative to the corner points of the 64-QAM constellation. The phase noise mask break points are at 1 kHz and 200 kHz. The average phase noise power is -29 dB relative to the carrier. The circles show the ideal performance curve.

- Performance degradation at SER $= 10^{-4}$ as caused by phase noise, is about 3 dB relative to the performance of an ideal system. This is identical to the value observed in Figs. 14 and 13.
- Phase estimation, and compensation using the CR algorithm shown in Fig. 5 results in an SER performance that is within 0.5 dB from ideal. This is about half the degradation suffered by the 8k OFDM system of Fig. 14.

Fig. 16 shows the symbol error rate as a function of the symbol energy to noise density ratio. These results are based on the simulation of an 8k OFDM system. The phase noise mask used here is similar to the one used in Fig. 6. From Fig. 16 it is clear that:

- The SER performance degradation due to channel estimation errors is relatively high by comparison to the degradation shown in the 8k OFDM case of Fig. 14. This increase is due to the use of 3 dB less power in the CE pilots.
- Performance degradation at SER $= 10^{-4}$, as caused by phase noise, is about 2.2 dB relative to the performance of an ideal system. This is lower than the value observed in Figs. 14 and 13. This reduction is due to the fact that the CE pilots an now lower and hence, they interfere less with the information symbols.
- Phase estimation and compensation using the CR algorithm shown in Fig. 5 results in an SER performance that is within 0.7 dB from ideal. This is about the same performance as shown in Fig. 14.

Fig. 17 shows the symbol error rate as a function of the symbol energy to noise density ratio. These results are based on the simulation of an 8k OFDM system. The phase noise mask used here is similar to the one used in Fig. 6. From Fig. 17 it is clear that:

- The SER performance degradation due to channel estimation errors is relatively high by comparison to the degradation shown in the 2k OFDM case of Fig. 15. This increase is due to the use of a 3 dB less power in the CE pilots.
- Performance degradation at SER $= 10^{-4}$, as caused by phase noise, is about 3 dB relative to the performance of an ideal system.
- Phase estimation and compensation using the CR algorithm shown in Fig. 5 results in an SER performance that is within 0.7 dB from ideal. This is slightly worse compared to the performance shown in Fig. 15.

Fig. 18 shows the symbol error rate as a function of the symbol energy to noise density ratio over a frequency selective channel. These results are based on the simulation of an

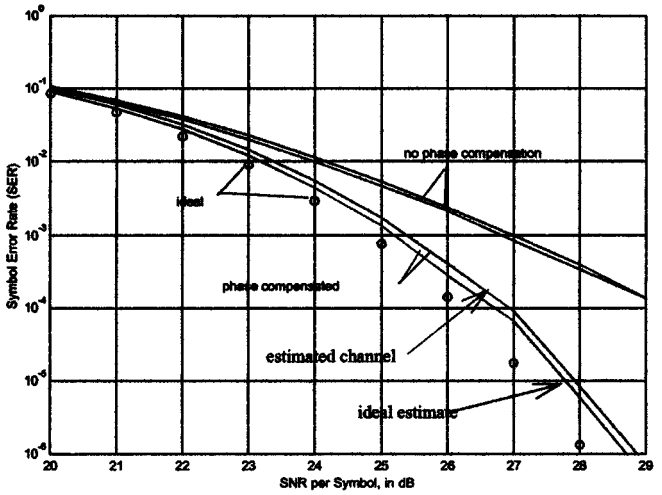

Fig. 15. SER performance of a 2048-tone OFDM system in the presence of phase noise over flat channels. This system uses 32 CE pilots at 6 dB relative to the comer points of the 64-QAM constellation. The phase noise mask break points are at 1 kHz end 200 kHz. The average phase noise power is -29 dB relative to the carrier. The circles show the ideal performance curve.

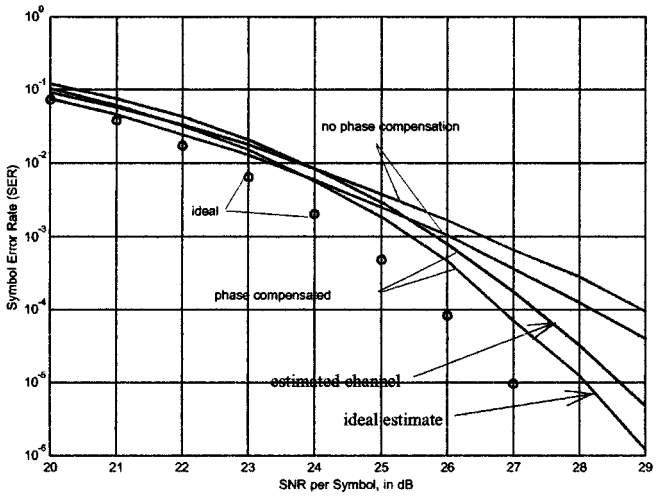

Fig. 16. SER performance of an 8192-tone OFDM system in the presence of phase noise over flat channels. This system uses 128 CE pilots at 3 dB relative to the corner points of the 64-QAM constellation. The phase noise mask break points are at 1 kHz and 200 kHz. The average phase noise power is -29 dB relative to the carrier. The circles show the ideal performance curve.

8k OFDM system. The phase noise mask used here is similar to the one used in Fig. 6. From Fig. 18, it is clear that:

- Performance degradation at SER $= 10^{-4}$, as caused by phase noise, is about 5 dB relative to the performance of art ideal system.
- Phase estimation and compensation using the CR algorithm shown in Fig. 5 results in an SER performance that is within 3.5 dB from ideal. This is much worse compared to the performance shown in Fig. 15. This may be explained by the fact that the ICI due to residual phase noise is enhanced due to the presence of powerful tones in the vicinity of weaker tones (the unevenness of tone power is caused by the frequency selectivity of the channel).

Fig. 19 shows the symbol error rate as a function of the symbol energy to noise density ratio over a frequency selective channel. These results are based on the simulation of an

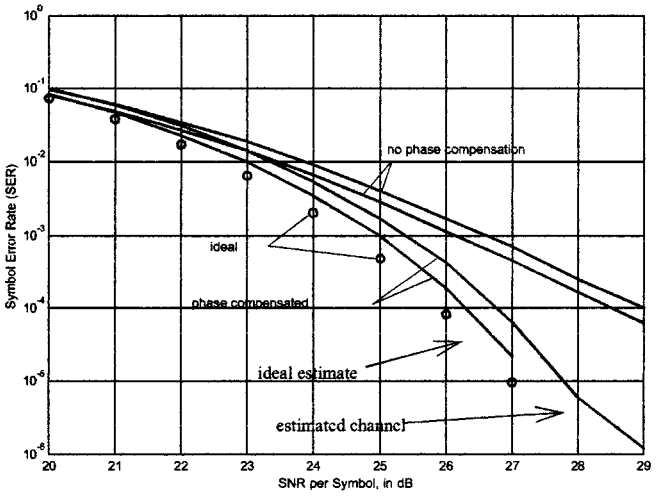

Fig. 17. SER performance of a 2048-tone OFDM system in the presence of phase noise, over flat channels. This system uses 32 CE pilots at 3 dB relative to the corner points of the 64-QAM constellation. The phase noise mask break points are at 1 kHz and 200 kHz. The average phase noise power is -29 dB relative to the carrier. The circles show an ideal performance curve for reference.

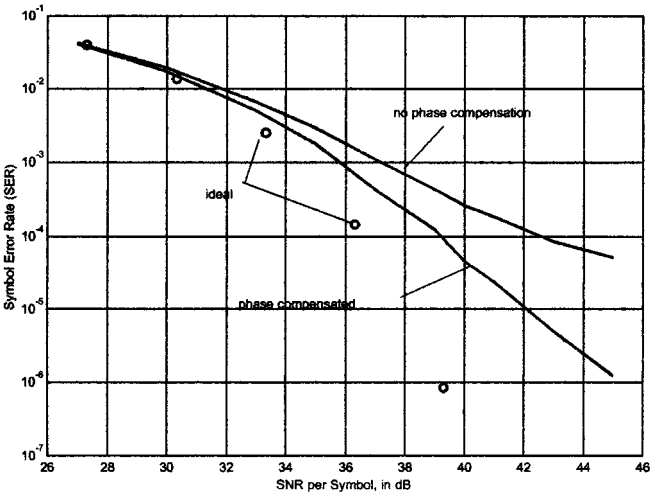

Fig. 18. SER performance of an 8192-tone OFDM system in the presence of phase noise over a frequency selective channel with impulse response $\mathrm{h} =$ [1 zeros(1, 7) j/2 zeros(1, 7) 1/4]. This system uses 128 CE pilots at 3 dB relative to the corner points of the 64-QAM constellation. The phase noise mask break points are at 1 kHz and 200 kHz. The average phase noise power is -29 dB relative to the carrier. The solid lines show performance based on the simulated channel and phase estimates. The circles show an ideal performance curve for reference.

2k OFDM system. The phase noise mask used here is similar to the one used in Fig. 6. From Fig. 19 it is clear that:

- Performance degradation at SER $= 10^{-4}$, as caused by phase noise, is about 5 dB relative to the performance of an ideal system.
- Phase estimation and compensation using the CR algorithm shown in Fig. 5 results in an SER performance that is within 1.2 dB from ideal. This is much better compared to the performance shown in Fig. 18. This may be explained by the fact that the ICI due to residual phase noise is less significant due to the fact that the tone spacing is now 4 times the tone spacing in the case of the 8k OFDM system, in spite of the unevenness of tone power.

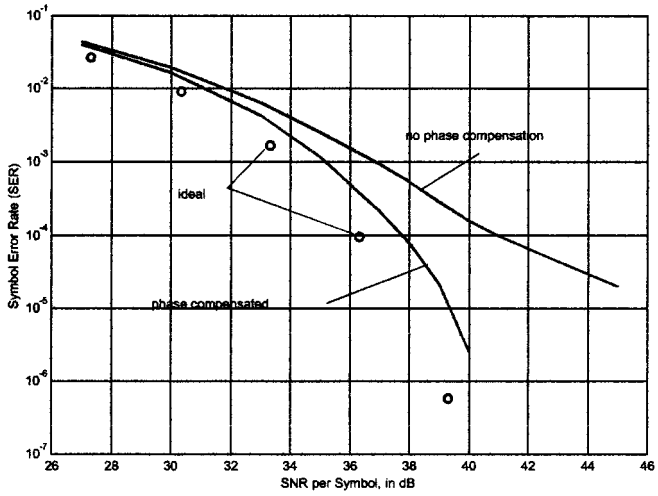

Fig. 19. SER performance of a 2048-tone OFDM system in the presence of phase noise over a frequency selective channel with impulse response $\mathrm{h} = [1\ 0\ 0\ \mathrm{j}/2\ 0\ 0\ 1/4]$. This system uses 32 CE pilots at 3 dB relative to the corner points of the 64-QAM constellation. The phase noise mask break points acre at 1 kHz and 200 kHz. The average phase noise power is -29 dB relative to the carrier. The solid lines show performance based on the simulated channel and phase estimates. The circles show an ideal performance curve for reference.

VIII. Conclusions

This paper presented an analytical procedure to quantify the impact of local oscillator phase noise on the performance of OFDM systems over additive white Gaussian noise channels. It also addressed the questions of performance over frequency selective channels. Based on simulation results, the paper also discussed the potential performance improvement that can be gained if the OFDM system employed a means of phase compensation on the receiving end. The impact of completely uncompensated phase noise is to create an irreducible error floor. Partial compensation for phase noise is also possible. The cases studied here indicate significant performance improvement in terms of SNR for both flat and for frequency selective channels.

Appendix
Derivation of BER in the Presence of Phase Noise

The M-QAM signal constellation is rectangular with constellation points represented by

$$\mathrm{p} = 1\delta + \mathrm{jm}\delta = \delta\sqrt{1^2+\mathrm{m}^2}\mathrm{e}^{\mathrm{j}atan(\mathrm{m/l})} \tag{A.1}$$

with $\{\mathrm{l}, \mathrm{m}\} = \{\pm1, \pm3, \pm5, \pm7\}$ for 64-QAM and $\{\mathrm{l}, \mathrm{m}\} = \{\pm1, \pm3\}$ for 16-QAM.

The impact of the phase noise process is modeled by multiplying the signal points above with the vector $\mathrm{e}^{\mathrm{jN_c}}$ to account for the rotational component, and by adding a noise component N_f to account for the dispersive component. This results in a decision variable with a mean

$$\begin{aligned}\tilde{\mathrm{p}} &= \mathrm{p}\mathrm{e}^{\mathrm{jN_c}} = \delta\sqrt{1^2+\mathrm{m}^2}\mathrm{e}^{\mathrm{j}(atan(\mathrm{m/l})+\mathrm{N_c})} \\ &= \delta[1\cdot cos\,\mathrm{N_c} - \mathrm{m}\cdot sin\,\mathrm{N_c}] + \mathrm{j}\delta[\mathrm{m}\cdot cos\,\mathrm{N_c} + 1\cdot sin\,\mathrm{N_c}]\end{aligned} \tag{A.2}$$

and a variance equal to the sum of the variances of the dispersive component and the variance of the additive thermal raise component. The decision variables can thus be written of the form

$$\mathrm{r} = \tilde{\mathrm{p}} + \mathrm{n_t} = \tilde{\mathrm{x}} + \mathrm{j}\tilde{\mathrm{y}} + \mathrm{n_{tr}} + \mathrm{jn_{ti}} = (\tilde{\mathrm{x}} + \mathrm{n_{tr}}) + \mathrm{j}(\tilde{\mathrm{y}} + \mathrm{n_{ti}}) \tag{A.3}$$

where n_t represents a complex Gaussian process which is equal to the sum of the additive noise and the dispersive component that is caused by the local oscillator phase noise process.

We note that the real and imaginary parts of r are independent Gaussian processes with equal variances. Their joint distribution is given by

$$\mathrm{P_r}\{\mathrm{x}, \mathrm{y}\} = \frac{1}{2\pi\sigma_\mathrm{t}^2} exp\left\{-\frac{(\mathrm{x}-\tilde{\mathrm{x}})^2}{2\sigma_\mathrm{t}^2}\right\} exp\left\{\frac{(\mathrm{y}-\tilde{\mathrm{y}})^2}{2\sigma_\mathrm{t}^2}\right\}. \tag{A.4}$$

To calculate the probability of error we divide the signal space into rectangular decision regions with boundaries at $(1\pm1)\delta$ and $(m\pm1)\delta$ for the inner constellation points. The outer points at the left, right, top or bottom of the constellation will have their respective decision regions extending to infinity on at least one side. With this in mind, we proceed to compute the average probability of error.

A. The Inner Constellation Points

For the inner constellation points the probability of making a correct decision is given by

$$\mathrm{P_c} = \int_{(\mathrm{l}-1)\delta}^{(\mathrm{l}+1)\delta} \mathrm{p_x}\,\mathrm{dx} \times \int_{(\mathrm{m}-1)\delta}^{(\mathrm{m}+1)\delta} \mathrm{p_y}\,\mathrm{dy} = \mathrm{P_1}\times\mathrm{P_2}. \tag{A.5}$$

The first integral above can be written as

$$\begin{aligned}\mathrm{P_1} &= \int_{(\mathrm{l}+1)\delta}^{(\mathrm{l}+1)\delta} \frac{1}{\sqrt{2\pi}\sigma_\mathrm{t}} exp\left\{-\frac{(\mathrm{x}-\tilde{\mathrm{x}})^2}{2\sigma_\mathrm{t}^2}\right\}\mathrm{dx} \\ &= \frac{1}{\sqrt{2\pi}}\int_{(-\delta+\delta\mathrm{mN_c})/\sigma_\mathrm{t}}^{(\delta+\delta\mathrm{mN_c})/\sigma_\mathrm{t}} \mathrm{e}^{-\eta^2/2}\,\mathrm{d}\eta \\ &= \tilde{\mathrm{P}}_1 - \Delta\tilde{\mathrm{P}}_1\end{aligned} \tag{A.6}$$

where

$$\tilde{\mathrm{P}}_1 = \frac{1}{\sqrt{2\pi}}\int_{-\delta/\sigma_\mathrm{t}}^{\delta/\sigma_\mathrm{t}} \mathrm{e}^{-\eta^2/2}\,\mathrm{d}\eta \tag{A.7}$$

and

$$\begin{aligned}\Delta\tilde{\mathrm{P}}_1 = &\frac{1}{\sqrt{2\pi}}\int_{(\delta/\sigma_\mathrm{t})(1-\mathrm{mN_c})}^{\delta/\sigma_\mathrm{t}} \mathrm{e}^{-\eta^2/2}\,\mathrm{d}\eta \\ &- \frac{1}{\sqrt{2\pi}}\int_{\delta/\sigma_\mathrm{t}}^{(\delta/\sigma_\mathrm{t})(1+\mathrm{mN_c})} \mathrm{e}^{-\eta^2/2}\,\mathrm{d}\eta.\end{aligned} \tag{A.8}$$

Similarly,

$$\begin{aligned}\mathrm{P_2} &= \int_{(\mathrm{m}-1)\delta}^{(\mathrm{m}+1)\delta} \frac{1}{\sqrt{2\pi}\sigma_\mathrm{t}} \exp\left\{\frac{(\mathrm{y}-\tilde{\mathrm{y}})^2}{2\sigma_\mathrm{t}^2}\right\}\mathrm{dx} \\ &= \frac{1}{\sqrt{2\pi}}\int_{(-\delta-\delta(1\cdot\mathrm{N_c}))/\sigma_\mathrm{t}}^{(\delta-\delta(1\cdot\mathrm{N_c}))/\sigma_\mathrm{t}} \mathrm{e}^{-\eta^2/2}\,\mathrm{d}\eta \\ &= \tilde{\mathrm{P}}_2 - \Delta\tilde{\mathrm{P}}_2\end{aligned} \tag{A.9}$$

where

$$\mathrm{P_2} = \frac{1}{\sqrt{2\pi}}\int_{-\delta/\sigma_\mathrm{t}}^{\delta/\sigma_\mathrm{t}} \mathrm{e}^{-\eta^2/2}\,\mathrm{d}\eta \tag{A.10}$$

and

$$\begin{aligned}\Delta\tilde{\mathrm{P}}_2 = &\frac{1}{\sqrt{2\pi}}\int_{(\delta/\sigma_\mathrm{t})(\mathrm{l}-1\cdot\mathrm{N_c})}^{\delta/\sigma_\mathrm{t}} \mathrm{e}^{-\eta^2/2}\,\mathrm{d}\eta \\ &- \frac{1}{\sqrt{2\pi}}\int_{(\delta/\sigma_\mathrm{t})(-\mathrm{l}-1\cdot\mathrm{N_c})}^{(-(\delta/\sigma_\mathrm{t}))} e^{-\eta^2/2}\,\mathrm{d}\eta.\end{aligned} \tag{A.11}$$

Therefore, the probability of error for an inner constellation point is given by

$$\mathrm{P_c} = (\tilde{\mathrm{P}}_1 - \Delta\tilde{\mathrm{P}}_1) \times (\tilde{\mathrm{P}}_2 - \Delta\tilde{\mathrm{P}}_2) = 1 - \mathrm{P_e} \tag{A.12}$$

where P_e can be written in the form

$$\mathrm{P_e} \cong \overline{\mathrm{P_e}} + \Delta\mathrm{P_e^i} \tag{A.13}$$

and

$$\begin{aligned}\Delta\mathrm{P_e} = &\int_{(\delta/\sigma_t)(1-1\cdot N_c)}^{\delta/\sigma_t} \frac{1}{\sqrt{2\pi}}\,\mathrm{e}^{-\eta^2/2}\,\mathrm{d}\eta \\ &- \int_{\delta/\sigma_t}^{(\delta/\sigma_t)(1+1\cdot N_c)} \frac{1}{\sqrt{2\pi}}\,\mathrm{e}^{-\eta^2/2}\,\mathrm{d}\eta \\ &+ \int_{(\delta/\sigma_t)(1-mN_c)}^{\delta/\sigma_t} \frac{1}{\sqrt{2\pi}}\,\mathrm{e}^{-\eta^2/2}\,\mathrm{d}\eta \\ &- \int_{\delta/\sigma_t}^{(\delta/\sigma_t)(1+mN_c)} \frac{1}{\sqrt{2\pi}}\,\mathrm{e}^{-\eta^2/2}\,\mathrm{d}\eta.\end{aligned} \tag{A.14}$$

B. The Exterior Constellation Points (Left/Right)

For the left/right exterior constellation points it can be shown that P_e is given by

$$\mathrm{P_e} \cong \overline{\mathrm{P_e}} + \Delta\mathrm{P_e^l} \tag{A.15}$$

where

$$\begin{aligned}\Delta\mathrm{P_e} = &\int_{-\delta/\sigma_f}^{-(\delta/\sigma_f)(1-mN_c)} \frac{1}{\sqrt{2\pi}}\,\mathrm{e}^{-\eta^2/2}\,\mathrm{d}\eta \\ &+ \int_{-(\delta/\sigma_f)(1-1\cdot N_c)}^{(\delta/\sigma_f)} \frac{1}{\sqrt{2\pi}}\,\mathrm{e}^{-\eta^2/2}\,\mathrm{d}\eta \\ &- \int_{\delta/\sigma_f}^{(\delta/\sigma_f)(1+1-N_c)} \frac{1}{\sqrt{2\pi}}\,\mathrm{e}^{-\eta^2/2}\,\mathrm{d}\eta.\end{aligned} \tag{A.16}$$

C. The Exterior Constellation Points (Top/Bottom)

For the top/bottom exterior constellation points it can be shown that P_e is given by

$$\mathrm{P_e} \cong \overline{\mathrm{P_e}} + \Delta\mathrm{P_e^t} \tag{A.17}$$

where

$$\begin{aligned}\Delta\mathrm{P_e} = &\int_{\delta/\sigma_f(1-mN_c)}^{\delta/\sigma_f} \frac{1}{\sqrt{2\pi}}\,\mathrm{e}^{-\eta^2/2}\,\mathrm{d}\eta \\ &- \int_{\delta/\sigma_f}^{\delta/\sigma_f(1+mN_c)} \frac{1}{\sqrt{2\pi}}\,\mathrm{e}^{-\eta^2/2}\,\mathrm{d}\eta \\ &- \int_{-(\delta/\sigma_f)(1+1\cdot N_c)}^{-(\delta/\sigma_f)} \frac{1}{\sqrt{2\pi}}\,\mathrm{e}^{-\eta^2/2}\,\mathrm{d}\eta.\end{aligned} \tag{A.18}$$

D. The Diagonal Constellation Points

For the diagonal constellation points it can be shown that $\mathrm{P_e}$ is given by

$$\mathrm{P_e} \cong \overline{\mathrm{P_e}} + \Delta\mathrm{P_e^d} \tag{A.19}$$

where

$$\begin{aligned}\Delta\mathrm{P_e} = &\int_{-\delta/\sigma_f}^{-\delta/\sigma_f(1-mN_c)} \frac{1}{\sqrt{2\pi}}\,\mathrm{e}^{-\eta^2/2}\,\mathrm{d}\eta \\ &- \int_{-\delta/\sigma_f(1+1\cdot N_c)}^{+\delta/\sigma_f} \frac{1}{\sqrt{2\pi}}\,\mathrm{e}^{-\eta^2/2}\,\mathrm{d}\eta.\end{aligned} \tag{A.20}$$

E. Conditional Probability of Error

The BER performance of 16-QAM OFDM and of 64-QAM OFDM for a given value of the rotational noise component N_c can now be written as follows:

$$\begin{aligned}&\mathrm{P_e}\big|_{16QAM} \\ &\quad = \overline{\mathrm{P}}_\mathrm{e} + \tfrac{3}{4}\left[(\Delta_1^1 - \Delta_2^1) + (\Delta_1^3 - \Delta_2^3)\right] \\ &\mathrm{P_e}\big|_{64QAM} \\ &\quad = \overline{\mathrm{P}}_\mathrm{e} + \tfrac{7}{16}\left[(\Delta_1^1 - \Delta_2^1) + (\Delta_1^3 - \Delta_2^3) + (\Delta_1^5 - \Delta_2^5)\right. \\ &\qquad\qquad \left. + (\Delta_1^7 - \Delta_2^7)\right]\end{aligned} \tag{A.21}$$

where

$$\begin{aligned}\Delta_1^1 &= \int_{(\delta/\sigma_f)(1-1\cdot N_c)}^{\delta/\sigma_f} \frac{1}{\sqrt{2\pi}}\,\mathrm{e}^{-\eta^2/2}\,\mathrm{d}\eta \\ \Delta_2^1 &= \int_{(\delta/\sigma_f)}^{(\delta/\sigma_f)(1-1\cdot N_c)} \frac{1}{\sqrt{2\pi}}\,\mathrm{e}^{-\eta^2/2}\,\mathrm{d}\eta\end{aligned} \tag{A.22}$$

and

$$\begin{aligned}\delta|_{16QAM} &= \sqrt{\frac{\mathrm{E_{av}}}{\mathrm{T_s}} \times \frac{3}{2\cdot(16-1)}} = \sqrt{\frac{\mathrm{E_{av}}}{10\cdot\mathrm{T_s}}} \\ \delta|_{64QAM} &= \sqrt{\frac{\mathrm{E_{av}}}{\mathrm{T_s}} \times \frac{3}{2\cdot(64-1)}} = \sqrt{\frac{\mathrm{E_{av}}}{42\cdot\mathrm{T_s}}}.\end{aligned} \tag{A.23}$$

Therefore,

$$\begin{aligned}\left.\frac{\delta}{\sigma_f}\right|_{16QAM} &= \sqrt{\frac{\mathrm{E_{av}}/\sigma_f^2}{10\cdot\mathrm{T_s}}} = \sqrt{\frac{\mathrm{SNR}}{10}} \\ \left.\frac{\delta}{\sigma_f}\right|_{64QAM} &= \sqrt{\frac{\mathrm{E_{av}}/\sigma_f^2}{42\cdot\mathrm{T_s}}} = \sqrt{\frac{\mathrm{SNR}}{42}}\end{aligned} \tag{A.24}$$

REFERENCES

[1] S. B. Weinstein and P. M. Ebert, "Data transmission by frequency division multiplexing using the discrete Fourier transform," *IEEE Trans. Commun.*, vol. COM-19, pp. 628–634, Oct. 1971.

[2] B. Le Floch, R. Halbert, and D. Castelain, "Digital sound broadcasting to mobile receivers," *IEEE Trans. Consumer Electronics*, vol. 35, pp. 493–503, Aug. 1989.

[3] J. J. Gledhill, S. V. Anikhindi, and P. A. Avon, "The transmission of digital television in the UHF baud using orthogonal frequency division multiplexing," in *IEE Sixth Int. Conf. Digital Processing of Signals in Commun.*, 1991, pp. 175–180.

[4] N. J. Fliege, "Orthogonal multiple carrier data transmission," in *European Trans. Telecomm. and related Technologies*, May–June 1992, pp. 255–263.

[5] A. Chini, M. S. El-Tanany, and S. A. Mahmoud, "Multi carrier modulation for indoor wireless communications," in *IEEE-ICUPC 93*, Oct. 1993, pp. 674–678.

[6] M. Alard and R. Lassalle, "Principles of modulation and channel coding for digital broadcasting for mobile receivers," *EBU Review—Technical*, no. 224, pp. 168–190, Aug. 1987.

[7] A. Chini, "Multi Carrier Modulation in Frequency Selective Fading Channels," Ph.D. dissertation, Carleton University, Canada, 1994.
[8] Claus Muschallik, "Influence of RF oscillators on an OFDM signal," *IEEE Trans. Consumer Electronics*, vol. 41, no. 3, pp. 592–603, August 1995.
[9] J. H. Stott, "The effects of phase noise in COFDM," BBC, R&D Department, Technical Note no. R&D 0127(94), Nov. 1994.
[10] J. H. Stott, "Phase noise in OFDM: Further insights, including the use of weighting functions," BBC, R&D Department Technical Note no. R&D 0166(94), Dec. 1994.

Mohammed S. El-Tanany obtained the B.Sc. and M.Sc. in electrical engineering in 1974 and 1978 respectively, both from Cairo University in Giza, Egypt, and the Ph.D. in electrical engineering from Carleton University, Ottawa, ON, Canada in 1983. He worked with the Advanced Systems division of Miller Communications in Kanata, Ontario from 1982 to 1985 with principal involvement in the research and development of digital transmission equipment for mobile satellite type of applications and also for VHF airborne high-speed down links. He joined Carleton University in 1985, initially as a research associate in the area of wireless communications for mobile and indoor communications. He is currently a professor with the Department of Systems and Computer Engineering where he is actively involved in several research programs that deal with digital transmission in the PCS and millimeter wave frequency bands, with emphasis on channel measurements, modeling as well as modulation/coding for frequency selective fading channels.

Yiyan Wu is a senior research scientist with the Communications Research Centre, Ottawa, Canada. His research interests include digital video compression and transmission, high definition television (HDTV), signal and image processing, satellite and mobile communications. He is actively involved in the ATSC technical and standard activities and ITU-R digital television and data broadcasting studies. He is an IEEE Fellow, an adjunct professor of Carleton University, Ottawa, Canada, a Member of the IEEE Broadcast Technology Society Administrative Committee and a member of the ATSC Executive Committee (representing IEEE).

László Házy obtained a B.Sc. in electronics and telecommunications from the Polytechnic Institute of Bucharest, Romania in 1992 and a M.Eng. in electrical engineering from Carleton University, Canada, in 1997. Currently he is a Ph.D. candidate at Carleton University. Between 1992 and 1995, he was an assistant professor with the Department of Electronics and Computers at Transilvania University, Romania, working in the area of radio and microwave communications. Between 1993 and 1995 he was also involved with the Research Institute for Computer Technology, Brasov, Romania. His research interests include digital communications theory and various aspects of wireless communication systems, and he is currently working on OFDM and multicarrier spread spectrum systems.